Grain boundary characterization in multicrystalline silicon using joint EBSD, EBIC, and atom probe tomography

Andreas Stoffers[1], Oana Cojocaru-Mirédin[1], Otwin Breitenstein[2], Winfried Seifert[3,4], Stefan Zaefferer[1], and Dierk Raabe[1]

[1] Max-Planck-Institut für Eisenforschung, Max-Planck-Straße 1, 40237 Düsseldorf, Germany
[2] Max-Planck-Institut für Mikrostrukturphysik, Weinberg 2, 06120 Halle/Saale, Germany
[3] Brandenburgische Technische Universität, Platz der Deutschen Einheit 1, 03046 Cottbus, Germany
[4] IHP, Im Technologiepark 25, 15236 Frankfurt (Oder), Germany

Abstract — The efficiency of multicrystalline silicon solar cells suffers from the presence of extended defects like dislocations and grain boundaries. In fact, the defects themselves do not implicitly have to be harmful, but their interaction with impurities makes them detrimental for the cell efficiencies.

Here, we present a systematic method to correlate the grain boundary charge recombination activity with local grain boundary properties and the site specific segregation information. For that, electron beam induced current is used to characterize the recombination activity at the grain boundaries, while electron backscatter diffraction is used to map the grain boundary crystallography. Atom probe tips containing the desired grain boundary are cut by using a novel site-specific sample preparation. Finally, atom probe tomography is used to reveal the 3D distribution of the impurities at the selected grain boundary.

In conclusion, this work is one of the first studies based on understanding the correlation between the charge recombination activity and structural as well as chemical properties at grain boundaries in multicrystalline silicon solar cells.

Index Terms — atom probe tomography, grain boundaries, impurities, recombination activity, multicrystalline silicon solar cells.

I. INTRODUCTION

Multicrystalline silicon (mc-Si) is a commonly used cost-effective bulk material for solar cell applications [1]. Up to date, the record efficiency registered for mc-Si solar cells is 20.4%, while the one registered for monocrystalline silicon solar cells is 25.0% [2]. Contrary to monocrystalline silicon, mc-Si contains high densities of defects such as dislocations, grain boundaries (GBs), and stacking faults, reducing the solar cell efficiency [1]. It is widely accepted that impurities play a major part in the electrical activity of the defects. According to Kveder et al. [3], the recombination activity of dislocations depends on the amount of transition metal contamination. Unfortunately, up to date our understanding of the electrical activity of GBs and its relation to structure and chemical composition (segregation) is still not satisfactory.

To develop a comprehensive understanding of the GB recombination activity, one needs to take all GB characteristics into account, including the local chemistry at the selected GB. Here, we performed a correlative EBSD-EBIC-APT analysis (EBSD: electron backscatter diffraction, EBIC: electron beam induced current, and APT: atom probe tomography) on a GB in mc-Si, since APT is the perfect tool for analyzing the amount and redistribution of the impurity elements at the GBs. Controlled field evaporation of the needle-shaped samples is achieved by applying a strong DC field and short laser pulses, as shown in fig. 1. Samples containing the GB of interest were prepared by using a novel joint Focused Ion Beam (FIB)-EBSD site-specific sample preparation procedure.

II. EXPERIMENTAL

The sample studied was taken from the capping region of a 200 mm mc-Si ingot. 20 ppm Fe and 20 ppm Cu were added during crystallization to study the influence of these impurity species on the electrical activity of the material. Prior studies on the same material revealed that this small amount of contamination is already detrimental for the solar cell efficiency [4].
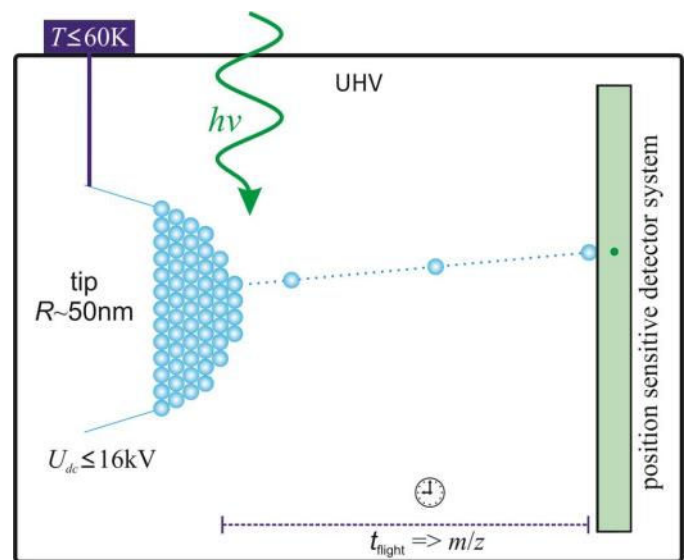

Fig. 1. Principle of Atom Probe Tomography.

The electrical characteristics were analyzed by conducting EBIC experiments at room temperature on the entire sample surface. Regions with high recombination activity show a low EBIC signal (dark region in the image) and are mostly connected to defects or precipitates. Electrically active GBs were studied in more detail on a smaller scale and interesting areas for further analysis were marked by Pt deposition in the FIB. Figure 2 a) shows a typical EBIC image with a strong recombination activity of several GBs. The formation of dot-shaped regions of dark contrast in the upper part might be due to the precipitation of impurities found in mc-Si bulk. In this study we focus on the recombination activity at GBs. Figure 2 b) provides an enlarged view of the marked area containing several GBs. The EBIC contrast is changing among GBs, but also within the same GB. We choose the area with strong EBIC contrast marked in yellow for further analysis. Here, site specific sample preparation for APT was done by Ga-ion milling on a FEI HeliosNanolab 600 dual beam FIB. We used the liftout method developed by Felfer [5] and added an additional step for the EBSD measurement. Indeed, a small

Fig. 3. TEM image of final APT tip with GB close to the apex.

lamella (approx. 20x2x2 µm³) is taken out and transformed into several tiny atom probe tips. During the liftout process we performed an EBSD scan on the lamella surface to characterize the local GB properties. In this way, 8 APT tips (M1-M8) were prepared from the shown sample area, where M1 was placed on the left-hand side of the dotted area and M8 was placed on the right-hand side. Before the annular milling of the APT tip, one side of each liftout segment was polished by low kV ion beam to have a smooth surface for the EBSD scan. The whole samples were then mounted on a special holder system to align the polished surfaces 70° relative to the electron beam in the SEM. Figure 2 c) shows an SEM image of one of the APT samples before the annular milling, overlaid with the EBSD information of the polished surface. By this, we are able not only to ensure that the liftout contains the desired GB, but also to get the local crystallographic information of the GB segment, which is analyzed in the APT at a later stage. This is a profound advantage, since the structural and chemical properties of the GB can change along the same boundary, e.g. in case of a curved interface or ledges [6].

After the EBSD measurement, a needle shaped tip is prepared out of the liftout by annular milling with the ion beam, as indicated by the dashed line in fig. 2 c). The same instrument was used for EBSD analysis and FIB liftout. EBSD scans were performed with a step size of 20 nm at 16 kV (electron beam) and the final FIB milling is performed at 5 kV (ion beam) to minimize the beam damage. Additionally, transmission electron microscopy (TEM) is performed on the final APT samples with a JEOL 2200 FS TEM operated at 200 kV. By this final TEM imaging (see fig. 3), we ensure that the GB of interest lies within the limited volume of analysis, very close to the apex of the needle shaped sample (approximately
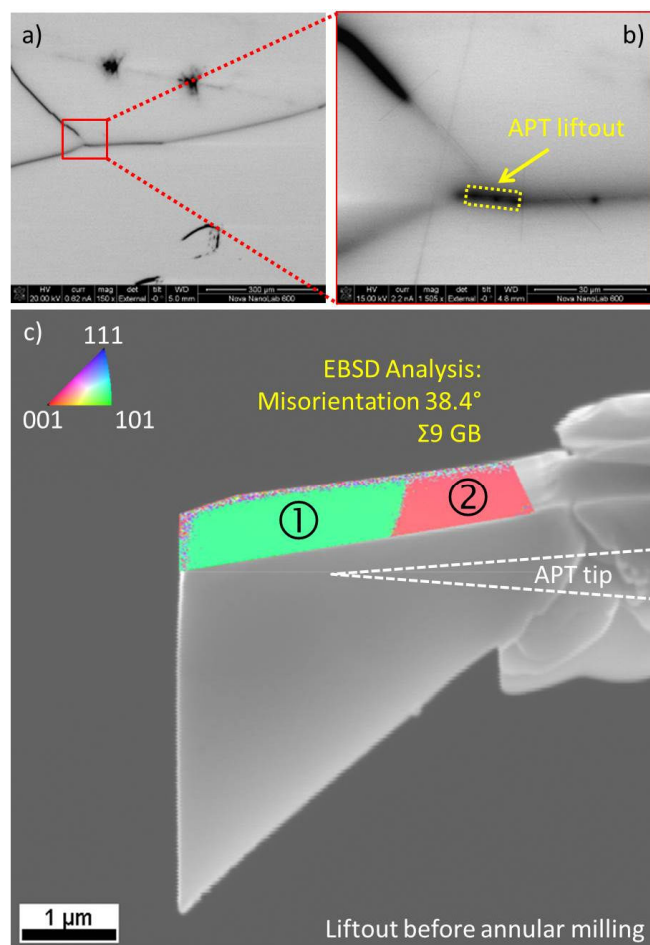

Fig. 2. a) EBIC map showing several GBs b) EBIC map of marked area with the liftout region marked by dashed rectangle c) overlay of SEM image of the liftout segment with EBSD map of the polished surface showing GB position
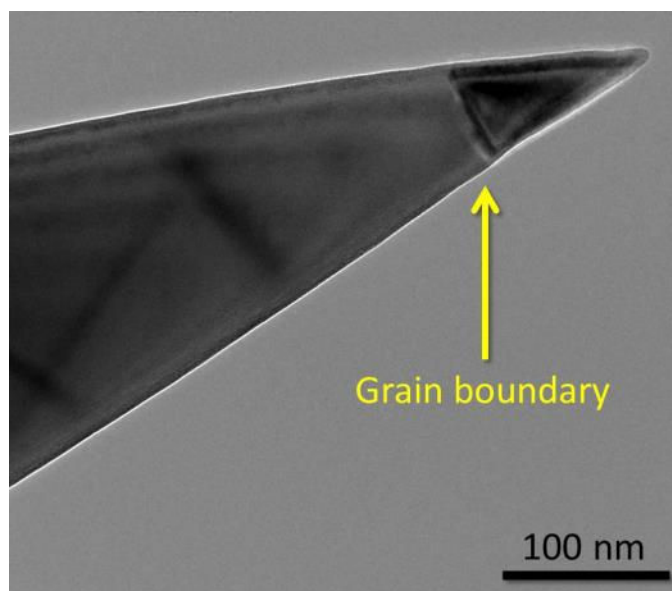
50-150 nm). Furthermore, the knowledge of the exact tip shape, e.g. tip radius, shank angle, and GB position enables a more accurate 3D reconstruction of the analyzed volume.

APT experiments were carried out on a local electrode atom probe (LEAPTM 3000X HR, Cameca Instruments) applying 12 ps laser pulses with energy of 0.35 nJ at a repetition rate of 160 kHz and a wavelength of 532 nm. The base temperature was set to 60K. The controlled field evaporation enables the chemical identification of the evaporated ions by the time of flight, whereas the position sensitive detector system enables the calculation of the coordinate of the evaporated ions. By this a full 3D reconstruction of the evaporated volume is achieved and we are able to detect, identify and quantify impurities in the vicinity of the GB.
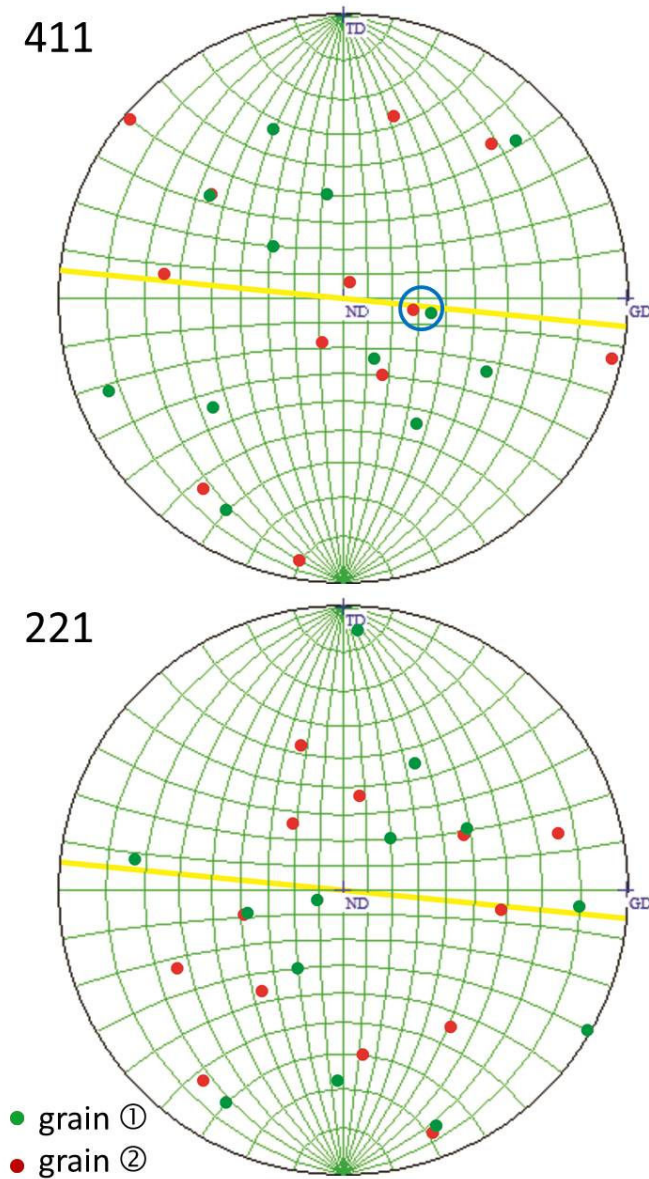

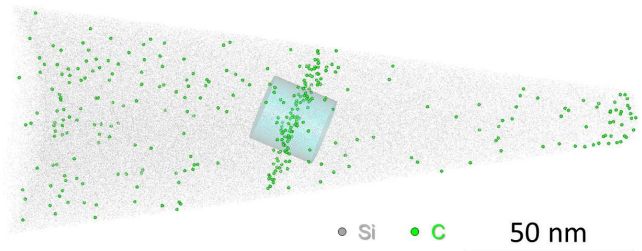Fig. 4.   Pole figures extracted from EBSD data to find the GB plane

Fig. 5.   Full 3D ion map from APT analysis. C atoms are plotted thicker for better visibility. A small cylinder is cut out for further analysis.

III. RESULTS

The EBSD map in fig. 2 c) clearly shows the GB position and identifies it as Σ9 CSL GB with a misorientation of 38.9°. We analyzed three different segments of the shown GB liftout, all of them showed the same GB characteristics. Due to geometrical reasons, we are not able to conduct EBSD experiments on the triangular shaped sample surface (front surface in fig. 2 c)). Therefore we cannot directly assess all crystallographic grain boundary parameters [7], but we can deduce the GB plane using the plane traces as follows: In fig. 4 the corresponding pole figures are plotted for the most common symmetrical Σ9 GB planes (221) and (411). The yellow line represents all possible GB normal vectors (perpendicular to the GB trace in fig. 2c)). In the (411) pole figure we find an overlap of planes from both grains with this yellow line, suggesting (411) as the most probably GB plane. The overlap is not perfect, what could indicate that the GB plane is slightly deviating from the perfectly symmetric situation.

Originally, we expected to detect the Fe or Cu distribution at this selected GB. However, in the time-of-flight spectra of the APT the signal of the dominating $^{56}Fe^{2+}$ isotope overlaps with the $^{28}Si^{1+}$ line and remains undetectable. There was also no significant Cu-related signal in the APT spectrum. This may be due to the fact that Cu is very mobile in Si even at room temperature. However, the spectrum contained a clear C-related signal. C is also a common impurity in solar silicon material. Though C itself is known not to be a dominant recombination center in Si, in the following the C distribution in this GB is investigated. Here C serves as a model impurity. It can be expected that GBs, which attract C due to their strain field, are also prone to attract Fe or other metallic recombination centers.

All three APT measurements of these GB segments show carbon segregation at the position of the GB, as can be seen in in fig. 5. The 3D ion map nicely shows segregation of C atoms along a straight line in a distance of 100 nm from the apex of the tip (the C atoms are plotted thicker for better visibility). This fits nicely to the GB-apex distance in the TEM image in fig. 3. We mention here, that the TEM image and the 3D ion map are not shown in the same orientation. The latter was rotated around the tip axis for better visibility of the GB segregation. Due to this, the inclination of the GB interface

with respect to the tip axis can be seen in the 3D ion map, but not in the TEM image. This inclination was already visible in the EBSD data in fig. 2 c).

To quantify the amount of C atoms segregated to the interface, we extract a small cylinder (R=20 nm, h=20 nm) containing the GB interface from the APT dataset for further analysis. The z-axis of the cylinder is aligned parallel to the GB normal direction. The 3D ion map of the extracted volume is shown in fig. 6 together with the corresponding 1D concentration profile of C along the cylinder z-axis. Locally, the C concentration is ∼0.2 at.% at the position of the GB interface. For comparison of different measurements the Gibbsian interfacial excess is a more adequate value, since it is not affected by possible artifacts which occur during the evaporation in APT (e.g. local magnification effects [8]). The Gibbsian interfacial excess gives the number of segregated atoms per area and can be extracted easily from the APT data by the method presented by Krakauer and Seidman [9]. The extracted values are shown in tab. 1. The calculation of the Gibbsian interfacial excess shows a high variance (see tab. 1), although all three samples were prepared from the same lamella where the GB character did not change significantly.
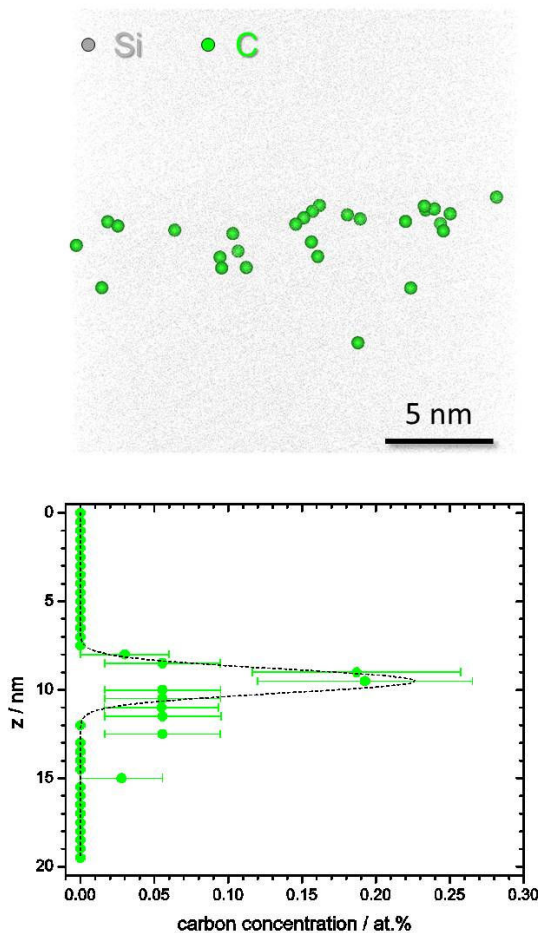

Fig. 6.   a) 3D ion map of small cylinder and b) corresponding 1D concentration profile of carbon along z-axis.

This big variance might be connected with a slight variance of the EBIC signal of the studied GB segment; the signal in the marked area in fig. 2 b) shows small dot-shaped spots within the dark GB signal. This variation in the EBIC contrast can have different reasons. It can be due to I) additional defects like dislocations, II) local variation in the impurity concentration, or III) a combination of I) and II) where regions with additional defects attract a higher number of impurities. Although it has been already shown in the literature that impurity enrichment can enhance the recombination activity at GBs [10], our present study cannot clearly elucidate whether defects or impurities are responsible for the increased activity observed for certain GBs. Therefore supplementary analyses are necessary in the future to solve this issue.

TABLE I
CALCULATED CARBON EXCESS

Tip	Gibbs' excess [10^{13} cm^{-2}]
M4	1.28
M6	2.25
M7	1.50

IV. CONCLUSION

In the present work we demonstrated the advantages of using several complementary characterization methods, namely, EBIC, EBSD, and APT for correlative GB characterization. We were able to identify and determine the amount of segregated impurity species at a GB with strong recombination activity. The presented APT data is one of the first direct measurements of impurities decorating GBs in mc-Si. The variance in the calculated excess values might be an explanation for the slight variance in the quantitative EBIC data. Furthermore, we were able to identify the analyzed GB as a Σ9 CSL boundary with the boundary plane being (411). All this information can help to get a deeper understanding of GB segregation in mc-Si. Due to our experience, not only the CSL character of a GB plays an important role in GB segregation, but also the boundary plane and coherency of the interface [7]. Further experiments with quantitative EBIC data are planned for better comparison and also the correlation with TEM experiments to be sensitive for defects like dislocations. Since we are not able to detect ^{56}Fe in Silicon, we intend to make similar investigations by using material artificially contaminated with Fe^{54}, which should be detectable.

ACKNOWLEDGEMENT

REFERENCES

[1]   M. Di Sabatino and G. Stokkan, "Defect generation, advanced crystallization, and characterization methods for high-quality solar-cell silicon," *physica status solidi (a),* vol. 210, pp. 641-648, 2013.

[2]   M. A. Green, K. Emery, Y. Hishikawa, W. Warta, and E. D. Dunlop, "Solar cell efficiency tables (version 43)," *Progress in Photovoltaics,* vol. 22, pp. 1-9, Jan 2014.

[3]   V. Kveder, M. Kittler, and W. Schröter, "Recombination activity of contaminated dislocations in silicon: A model describing electron-beam-induced current contrast behavior," *Physical Review B,* vol. 63, 2001.

[4]   S. Riepe, I. E. Reis, W. Kwapil, M. A. Falkenberg, J. Schön, H. Behnken*, et al.*, "Research on efficiency limiting defects and defect engineering in silicon solar cells - results of the German research cluster SolarFocus," *physica status solidi (c),* vol. 8, pp. 733-738, 2011.

[5]   P. J. Felfer, T. Alam, S. P. Ringer, and J. M. Cairney, "A reproducible method for damage-free site-specific preparation of atom probe tips from interfaces," *Microsc Res Tech,* vol. 75, pp. 484-91, Apr 2012.

[6]   M. Herbig, D. Raabe, Y. J. Li, P. Choi, S. Zaefferer, and S. Goto, "Atomic-Scale Quantification of Grain Boundary Segregation in Nanocrystalline Material," *Physical Review Letters,* vol. 112, Mar 27 2014.

[7]   S. Mandal, K. G. Pradeep, S. Zaefferer, and D. Raabe, "A novel approach to measure grain boundary segregation in bulk polycrystalline materials in dependence of the boundaries' five rotational degrees of freedom," *Scripta Materialia,* vol. 81, pp. 16-19, 2014.

[8]   F. Vurpillot, A. Cerezo, D. Blavette, and D. J. Larson, "Modeling image distortions in 3DAP," *Microscopy and Microanalysis,* vol. 10, pp. 384-390, Jun 2004.

[9]   B. W. Krakauer and D. N. Seidman, "Absolute Atomic-Scale Measurements of the Gibbsian Interfacial Excess of Solute at Internal Interfaces," *Physical Review B,* vol. 48, pp. 6724-6727, Sep 1 1993.

[10]   B. Chen, J. Chen, T. Sekiguchi, M. Saito, and K. Kimoto, "Structural characterization and iron detection at Sigma 3 grain boundaries in multicrystalline silicon," *Journal of Applied Physics,* vol. 105, Jun 1 2009.